Nonlinear Analysis of GaN MESFETs With Volterra Series Using Large-Signal Models Including Trapping Effects

Syed S. Islam, *Student Member, IEEE,* and A. F. M. Anwar, *Senior Member, IEEE*

***Abstract*—Nonlinearities in GaN MESFETs are reported using a large-signal physics-based model. The model accounts for the observed current collapse to determine the frequency dispersion of output resistance and transconductance. Calculated f_T and $f_{\max}$ of a 0.8 μm $\times$ 150 μm GaN MESFET are 6.5 and 13 GHz, respectively, which are in close agreement with their measured values of 6 and 14 GHz, respectively. A Volterra-series technique is used to calculate size and frequency-dependent nonlinearities. For a 1.5 μm $\times$ 150 μm FET operating at 1 GHz, the 1-dB compression point and output-referred third-order intercept point are 16.3 and 22.2 dBm, respectively. At the same frequency, the corresponding quantities are 19.6 and 30.5 dBm for a 0.6 μm $\times$ 150 μm FET. Similar improvements in third-order intermodulation for shorter gatelength devices are observed.**

***Index Terms*—GaN MESFETs, large-signal modeling, Volterra series and intermodulation distortion.**

I. Introduction

RECENTLY, GaN-based devices are being pursued extensively for potential applications in high-power microwave circuitries. GaN with a bandgap of 3.4 eV and a breakdown field of 4 MV/cm allows GaN-based devices to operate with higher supply voltage to provide higher output power as compared to similar channel-length GaAs and Si FETs [1]. Besides, superior transport characteristics in terms of electron peak velocity (3×10^7 cm/s), saturation velocity (1.5×10^7 cm/s), low field mobility (1500 cm^2/V $\cdot$ s) [2], and lower parasitic is suitable for high-frequency applications, as has recently been reported by Lu *et al.* [3], where $f_T = 101$ GHz and $f_{\max} = 155$ GHz were obtained with a 0.12 μm $\times$ 100 μm GaN/$Al_{0.20}Ga_{0.80}N$ high electron-mobility transistor (HEMT). GaN grown on SiC offers a thermal conductivity of 4.5 W/cm $\cdot$ K, making the system suitable for high-temperature and high-power applications. Consequently, output power of 9.8 W/mm at 8 GHz has been reported by Wu *et al.* [4] using a 0.5 μm $\times$ 150 μm $Al_{0.38}Ga_{0.62}N$/GaN HEMT. Moreover, Daumiller *et al.* [5] have reported GaN-based FETs with operating up to 750 C.

With improved growth and fabrication techniques, device fabrication is progressing at a frantic pace. However, this has not been followed by comparable effort in modeling. The optimization of the power-handling capability, especially at higher frequencies, requires nonlinear analysis using large-signal transistor models [6], [7]. Moreover, the large-signal device models used in microwave circuitries must include dc-to-RF dispersions of the device characteristics for accurate analysis of the analog- and mixed-signal and high-power circuits [8], [9]. The dispersion of the electrical characteristics, especially the device transconductance and output resistance, are due to the presence of traps in the structure. Recently, quite a few authors have reported the effect of traps on the current collapse in the dc current–voltage characteristics. Binari *et al.* [10] have demonstrated that the application of a moderately large drain bias (up to 10 V) did not result in current collapse in a GaN HEMT. However, the application of a drain bias exceeding 20 V results in current collapse in the subsequent measurements. A similar observation has been reported by Hsin *et al.* [11] for a GaN/InGaN heterojunction field-effect transistor (HFET). Current collapse is observed in the absence of light and is associated with the trapping of electrons at the channel/buffer interface [12]. Kunihiro *et al.* [13] have reported recovery of current collapse with measurements carried out with 10-s hold time, which relates trapping effects with the applied signal frequency and can be modeled by the frequency dispersion of device transconductance and output resistance [8], [9]. Based upon these observations, a mechanism to explain current collapse in GaN MESFETs is proposed and a physics-based model to incorporate dc-to-RF dispersion of transconductance and output resistance is developed [14], [15]. The dispersion frequency depends on the detrapping time constant and increases with increasing temperature. For GaN-based devices, dispersion frequency is of the order of hertz at room temperature; however, it increases to the megahertz range at 600 K [14]. Thus, the device transconductance and output resistance obtained at dc should be corrected to include the dispersion effects for microwave circuit analysis.

In this paper, nonlinearities in GaN MESFET have been analyzed using a Volterra-series technique. Volterra-series analysis, a frequency-domain technique, has been extensively used for nonlinear analysis of GaN HEMTs [6], GaAs MESFETs [16], and AlGaAs/GaAs heterojunction bipolar transistors (HBTs) [17]. A large-signal physics-based model is used in this analysis, which takes into account the frequency dispersion of transconductance and output resistance. The size dependence of 1-dB compression points $(P_{1\text{-dB}})$, output-referred third-order

Manuscript received April 5, 2002.

S. S. Islam is with the Department of Electrical Engineering, Rochester Institute of Technology, Rochester, NY 14623 USA.

A. F. M. Anwar is with the Department of Electrical and Computer Engineering, University of Connecticut, Storrs, CT 06269-2157 USA (e-mail: anwara@engr.uconn.edu).

Digital Object Identifier 10.1109/TMTT.2002.804518

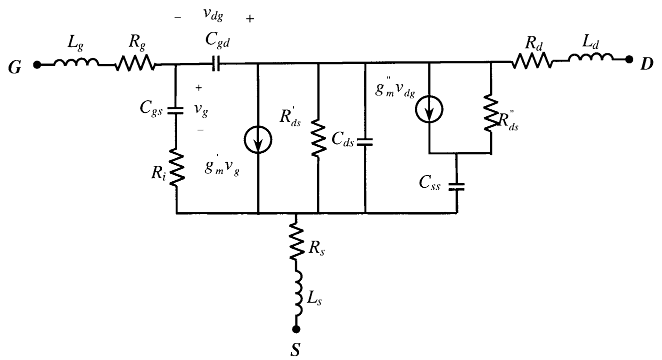

Fig. 1. GaN MESFET large-signal model. Linear model parameters are $R_g = 6\ \Omega$, $L_g = 0.055$ nH, $R_d = 70\ \Omega$, $L_d = 0.307$ nH, $R_s = 90\ \Omega$, $L_s = 0.027$ nH, $R_i = 25\ \Omega$, and $C_{\rm ds} = 0.040$ pF [8], [12].

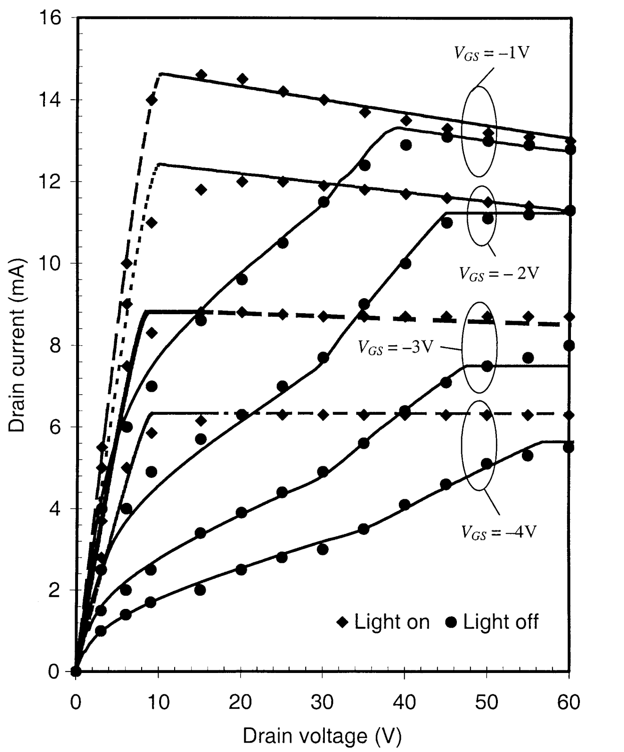

Fig. 2. *I–V* characteristics considering trapping effects of the 1.5 μm × 150 μm GaN MESFET [12]. Calculated and measured results are shown by solid lines and symbols, respectively.

intercept points (OIP3s) and third-order intermodulation points (IM3s) is analyzed.

II. Analysis

The large-signal GaN MESFET circuit model is shown in Fig. 1. Following the treatment reported by Golio *et al.* [8], $g''_m, R''_{\rm ds}$, and $C_{\rm ss}$ are incorporated in the intrinsic MESFET equivalent circuit to account for the frequency dispersion of transconductance and output resistance due to traps. Expressions of these circuit parameters are given in the Appendix and are based upon the incorporation of traps to determine the current–voltage characteristics [14], [15]. In Fig. 2, the calculated *I–V* characteristics for a 1.5 μm × 150 μm GaN MESFET [12] with channel thickness $d = 2000$ Å, channel doping $N_d = 2 \times 10^{17}$ cm^{-3}, trap concentration at the channel–buffer inter-

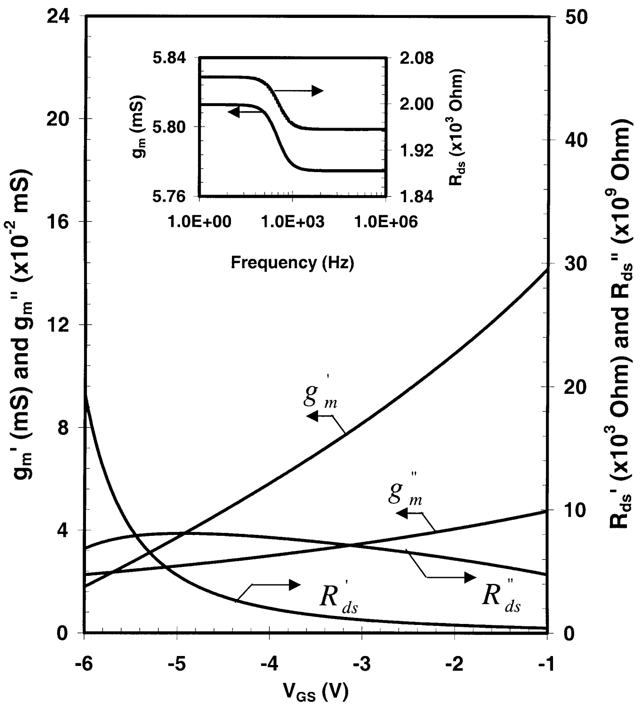

Fig. 3. Transconductances (g'_m and g''_m) and resistances ($R'_{\rm ds}$ and R''_{ds}) as a function of gate voltage with $V_{\rm DS} = 25$ V for the 1.5 μm × 150 μm GaN MESFET [12]. Inset shows the intrinsic transconductance (g_m) and output resistance ($R_{\rm ds}$) as a function of frequency for $V_{\rm DS} = 25$ V, $V_{\rm GS} = -4$ V, and $t_d = 0.5$ ms.

face $N_{\rm to} = 1.5 \times 10^{16}$ cm^{-3}, and low field mobility $\mu_n = 410$ cm^{2}V^{-1}s^{-1} are shown. In this same figure, experimental results are also plotted to show good agreement. The agreement is achieved by assuming exponential decay of the occupied trap density in the form $N_t = N_{\rm to}\exp(-\alpha(V_{\rm DS} - V_{\rm DS}^{\rm ONSET}))$, where $V_{\rm DS}^{\rm ONSET}$ is the drain bias at first pinchoff with all the traps being occupied and $\alpha = 0.112$ V^{-1}.

Fig. 3 shows the variation of $g'_m, g''_m, R'_{\rm ds}$ and $R''_{\rm ds}$ as a function of gate bias for a 1.5 μm × 150 μm GaN MESFET at $V_{\rm DS} = 25$ V [12]. g'_m and $R'_{\rm ds}$ follow variations of device transconductance and output resistance with gate bias typical to any standard MESFET. For a detrapping time constant t_d of 0.5 ms [14], $R''_{\rm ds}$ is of the order of $10^9\ \Omega$ and much higher than the other resistive components in the model. The variation of the overall intrinsic transconductance and output resistance with increasing frequency is shown as an inset in Fig. 3. At low frequency, the overall intrinsic transconductance g_m equals g'_m, whereas for frequencies greater than the dispersion frequency, $f_{o(gm)} = 1/2\pi C_{\rm ss} R''_{\rm ds}, g_m$ approaches $g'_m - g''_m$. For frequencies lower than $f_{o({\rm rds})} = 1/2\pi t_d$, the overall output resistance approaches $R'_{\rm ds}$ and becomes $R'_{\rm ds} \| R''_{\rm ds} \| 1 g''_m$ for frequencies greater than $f_{o({\rm rds})}$ [14]. The other intrinsic circuit parameters are obtained by conventional small-signal MESFET analysis.

For large-signal analysis, g_m, $g_{\rm ds}$, and $C_{\rm gs}$ are considered nonlinear functions of v_g, while $C_{\rm gd}$ is nonlinear function of $v_{\rm dg}$. The nonlinear functions are approximated up to the second-order term $p = p_0 + p_1 v + p_2 v^2$, where p represents g_m, $g_{\rm ds}$, $C_{\rm gs}$, or $C_{\rm gd}$ and v represents v_g or $v_{\rm dg}$. The coefficients p_0, p_1, and p_2 are shown in Table I for $L \times 150$ μm GaN MESFETs at $V_{\rm DS} = 25$ V.

TABLE I
NONLINEAR MODEL PARAMETERS FOR $L \times 150$ μm GaN MESFETs (v_g OR $v_{\rm dg}$ ARE IN VOLTS AND $V_{\rm DS} = 25$ V) [12]

	$L = 0.6\mu$m	$L = 0.8\mu$m	$L = 1.0\mu$m	$L = 1.5\mu$m
g_{m0} (mS)	43.4	32.5	26.0	17.3
g_{m1} (mS.V^{-1})	8.8	6.6	5.3	3.5
g_{m2} (mS.V^{-2})	0.40	0.30	0.24	0.16
g_{ds0} (mS)	8.5	6.4	5.1	3.4
g_{ds1} (mS.V^{-1})	2.7	2.0	1.6	1.1
g_{ds2} (mS.V^{-2})	0.21	0.16	0.13	0.09
C_{gs0} (fF)	133.6	178.2	222.7	334.1
C_{gs1} (fF.V^{-1})	25.0	33.4	41.7	62.5
C_{gs2} (fF.V^{-2})	2.10	2.80	3.50	5.25
C_{gd0} (fF)	21.5	28.7	35.9	53.8
C_{gd1} (fF.V^{-1})	–0.49	–0.66	–0.82	–1.23
C_{gd2} (fF.V^{-2})	0.005	0.007	0.009	0.013

Defining ports 1–5 across nonlinear elements $C_{\rm gs}, g_m$ and $g_{\rm ds}, C_{\rm gd}$, load and source, respectively, and terminating the source and load with impedances Z_S and Z_L, respectively, the elements of the 5×5 system matrix Y are expressed as follows:

$$Y_{1,1}(\omega) = 1/R_i + j\omega C_{\rm gs0} \tag{1}$$

$$Y_{1,2}(\omega) = Y_{1,3}(\omega) = Y_{3,1}(\omega) = -1/R_i \tag{2}$$

$$Y_{2,1}(\omega) = -1/R_i + g_{m0} \tag{3}$$

$$Y_{1,4}(\omega) = Y_{4,1}(\omega) = Y_{1,5}(\omega) = Y_{5,1}(\omega) = 0 \tag{4}$$

$$Y_{2,2}(\omega) = 1/R_i + \Big[\big\{1/(R_d + j\omega L_d) + 1/(Z_s(\omega) + R_g + j\omega L_g)\big\}^{-1} + R_s + j\omega L_s\Big]^{-1} + j\omega C_{\rm ds} + g_{\rm ds0} \tag{5}$$

$$Y_{4,4}(\omega) = \Big[\big\{1/(Z_s(\omega) + R_g + j\omega L_g) + 1/(R_s + j\omega L_s)\big\}^{-1} + R_d + j\omega L_d\Big]^{-1} + 1/Z_L(\omega) \tag{6}$$

$$Y_{5,5}(\omega) = \Big[\big\{1/(R_s + j\omega L_s) + 1/(R_d + j\omega L_d)\big\}^{-1} + Z_s(\omega) + R_g + j\omega L_g\Big]^{-1} \tag{7}$$

$$Y_{2,5}(\omega) = Y_{5,2}(\omega) = -Y_{5,5}(\omega)\Big[(R_d + j\omega L_d)/(R_s + j\omega L_s + R_d + j\omega L_d)\Big] \tag{8}$$

$$Y_{2,4}(\omega) = Y_{4,2}(\omega) = \Big[1/Z_L(\omega) - Y_{4,4}(\omega)\Big] \times \left[\frac{Z_s(\omega) + R_g + j\omega L_g}{R_s + j\omega L_s + Z_s(\omega) + R_g + j\omega L_g}\right] \tag{9}$$

$$Y_{3,4}(\omega) = Y_{4,3}(\omega) = \Big[Y_{4,4}(\omega) - 1/Z_L(\omega)\Big] \times \left[\frac{R_s + j\omega L_s}{R_s + j\omega L_s + Z_s(\omega) + R_g + j\omega L_g}\right] \tag{10}$$

$$Y_{2,3}(\omega) = Y_{3,2}(\omega) = 1/R_i - Y_{2,5}(\omega) \tag{11}$$

$$Y_{3,3}(\omega) = Y_{5,5}(\omega) + 1/R_i + j\omega C_{\rm dg0} \tag{12}$$

$$Y_{3,5}(\omega) = Y_{5,3}(\omega) = -Y_{5,5}(\omega) \tag{13}$$

$$Y_{5,4}(\omega) = Y_{4,5}(\omega) = -Y_{3,4}(\omega). \tag{14}$$

With an applied signal of amplitude V_{s1} at frequency ω_1, the first-order port voltages across ports 1–4 are determined by using the following matrix equation [18]:

$$\big[V_p(\omega_1)\big] = -\big[Y_{i=p,j=1,\ldots,4}\big]^{-1}\big[Y_{i=p,j=5}\big]^T\big[V_{5,1} = V_{s1}\big], \quad p = 1, \ldots, 4. \tag{15}$$

Second-order voltages $V_p(\omega_1, \omega_2)$ appear across ports at mixing frequency $\omega_1 + \omega_2$ when two tones are applied with amplitudes V_{s1} and V_{s2} at frequencies ω_1 and ω_2, respectively. Second-order port voltages are calculated by applying nonlinear currents through each nonlinear port. The nonlinear currents are evaluated by using the first-order port voltages due to individual tones and p_1 coefficients of the nonlinear elements [18]. With the Y matrix evaluated at mixing frequencies, the second-order port voltages are obtained by solving the following matrix equation:

$$\big[V_p(\omega_1, \omega_2)\big] = -\big[Y_{i=p,j=1,\ldots,4}\big]^{-1}\big[I_{i=p,2}\big]^T, \quad p = 1, \ldots, 4. \tag{16}$$

Similarly, third-order port voltages $V_p(\omega_1, \omega_2, \omega_3)$ due to tone amplitudes V_{s1}, V_{s2} and V_{s3} at frequencies ω_1, ω_2 and ω_3, respectively, are calculated by using the first- and second-order port voltages and nonlinear coefficients p_1 and p_2. The first-, second-, and third-order transfer functions are expressed as follows:

$$H_1(\omega_1) = V_4(\omega_1)/\big[V_{s1} Z_L(\omega_1)\big] \tag{17}$$

$$H_2(\omega_1, \omega_2) = 2\frac{V_4(\omega_1, \omega_2)}{V_{s1} V_{s2} Z_L(\omega_1, \omega_2)} \tag{18}$$

$$H_3(\omega_1, \omega_2, \omega_3) = 4\frac{V_4(\omega_1, \omega_2, \omega_2)}{V_{s1} V_{s2} V_{s3} Z_L(\omega_1, \omega_2, \omega_3)}. \tag{19}$$

With two equal amplitude tones at frequencies ω_1 and ω_2, the third-order intermodulation components appear at $2\omega_1 - \omega_2$ and $2\omega_2 - \omega_1$. The output power and third-order intermodulation distortion are as follows:

$$P_{\rm out} = 0.5\big|V_4(\omega_1)/Z_L(\omega_1)\big|^2 {\rm Re}\big[Z_L(\omega_1)\big] \tag{20}$$

and

$$\text{IM3} = 20\log_{10}\left[\frac{3}{4} V_{s1} V_{s2} \frac{|H_3(\omega_1, \omega_1, -\omega_2)|}{|H_1(\omega_1)|}\right]. \tag{21}$$

III. RESULTS AND DISCUSSION

Fig. 4 shows the calculated short-circuit current gain $|h_{21}|$, maximum stable gain (MSG), and maximum available gain (MAG) for a 0.8 μm $\times$ 150 μm GaN MESFET. The calculated results are compared with experimental data to show good agreement. $|h_{21}|$ is 29 dB at 0.2 GHz and drops to 0 dB at 6.5 GHz, which corresponds to the unity gain current cutoff frequency f_T. MAG drops to 0 dB at 13 GHz and corresponds to the maximum frequency of oscillation $f_{\max}$ of the device. Inset shows the calculated f_T and $f_{\max}$ with increasing gate length. Experimental results for f_T are also plotted to show agreement. A steady increase in f_T for shorter gatelength devices is due to the increase in the overall transconductance along with a decrease in the gate–source and gate–drain capacitances.

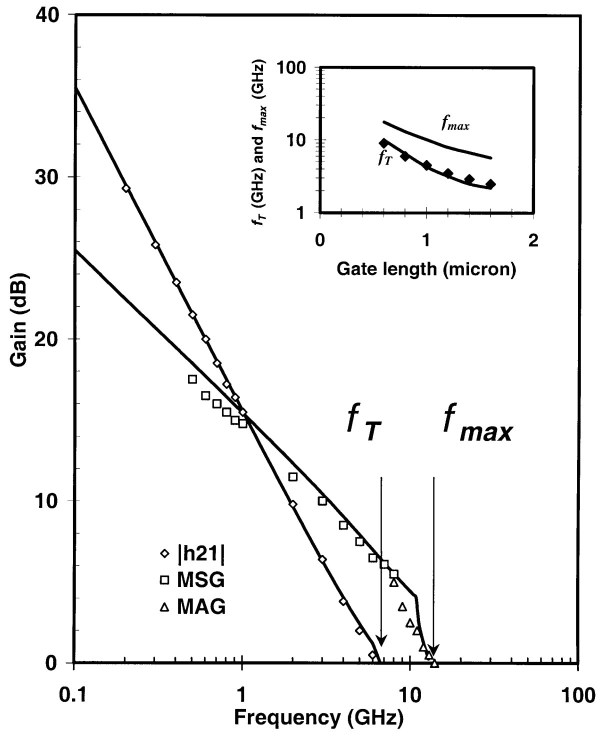

Fig. 4. Calculated (solid lines) and measured (symbol) short-circuit current gain $|h_{21}|$, MSG, and MAG of an 0.8 μm $\times$ 150 μm GaN MESFET. Inset shows the variation of f_T and $f_{\max}$ with gate length ($V_{\rm GS} = -4$ V and $V_{\rm DS} = 25$ V) [12] (experimental data is shown by a symbol).

Fig. 5 shows the fundamental and third-order output powers as a function of input power with gate length as a parameter with tones at 1 and 1.01 GHz. The source and load resistances are 50 Ω each. With increasing input power, the fundamental component of the output power becomes sub-linear as the power delivered to the higher harmonics increases due to increasing device nonlinearity. The observed gatelength dependence is explained as follows. As shown in Table I, with decreasing gate length, g_{m0} increases and $C_{\rm gs0}$ decreases, which results in higher first-order transfer function $|H_1(\omega_1)|$ of the device. Thus, for a given input power, the fundamental component of the output power increases for shorter lengths. However, with decreasing gate length, the third-order transfer function $|H_3(\omega_1, \omega_1, -\omega_2)|$ decreases due to decreasing $C_{\rm gd}$. Consequently, a lower third-order component of the output power is observed for shorter gatelength devices.

A 1-dB compression point $(P_{1\text{-dB}})$ is referred to as the input power at which output power deviates from linearity by 1 dB. The OIP3 is defined as the output power at which the third-order intermodulation component of the output power intersects the fundamental component. Fig. 6. shows the variation of $P_{1\text{-dB}}$ and OIP3 with increasing gate length. $P_{1\text{-dB}}$ for a 1.5-μm gatelength device is 16.3 dBm, which increases to 19.6 dBm for a MESFET with 0.6-μm gate. The respective OIP3s are 22.2 and 30.5 dBm. These results are due to the significant improvement in device linearity for shorter gatelength devices. A similar result is reported for GaN/AlGaN HEMTs [7].

Fig. 7 shows the third-order intermodulation distortion (i.e., IM3) as a function of output power for varying gate lengths with tones at 1 and 1.01 GHz. The source and load resistances are

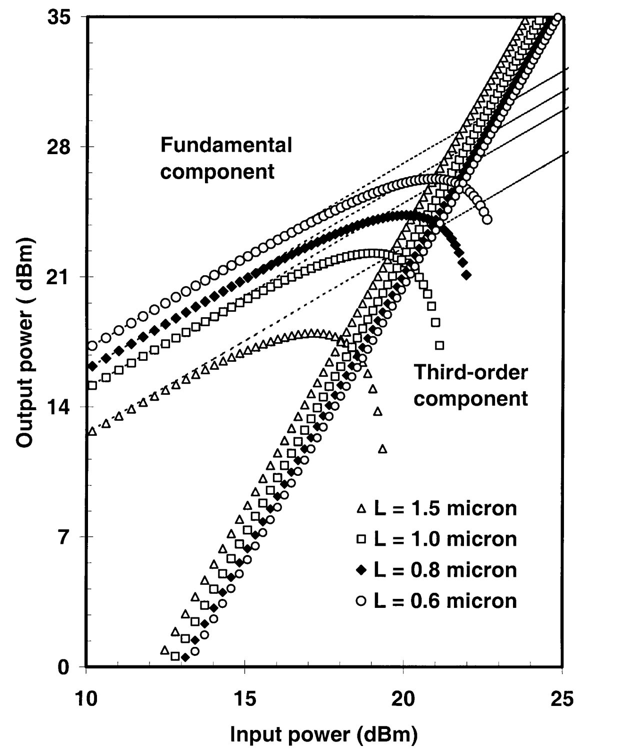

Fig. 5. Calculated fundamental and third-order components of output power of $L \times 150$ μm GaN MESFETs ($V_{\rm GS} = -4$ V and $V_{\rm DS} = 25$ V) [12].

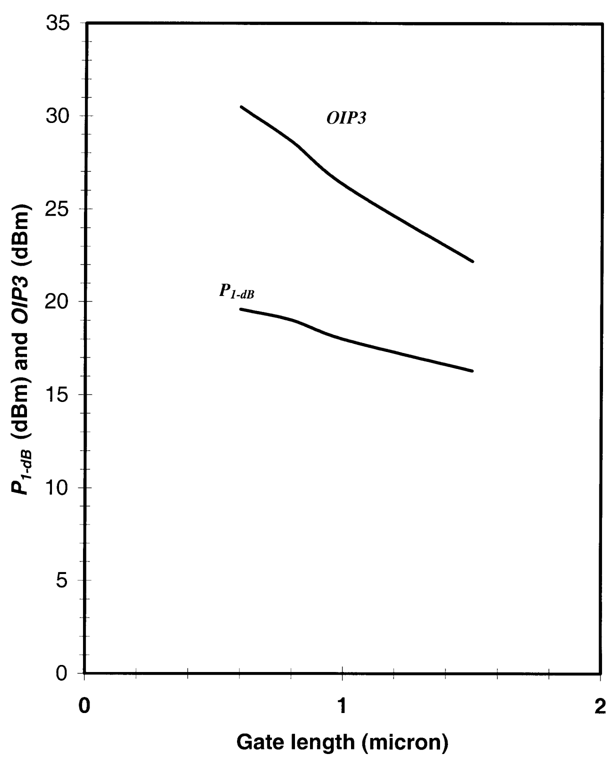

Fig. 6. 1-dB compression point $(P_{1\text{-dB}})$ and OIP3 as a function of gate length ($V_{\rm GS} = -4$ V and $V_{\rm DS} = 25$ V) [12].

50 Ω each. At 20-dBm output power, IM3 for a 0.6-μm gatelength device is -30 dBc and increases to -14.13 dBc for the 1.5-μm gatelength device. This is due to the improvement in device linearity for shorter gatelength devices, as explained above.

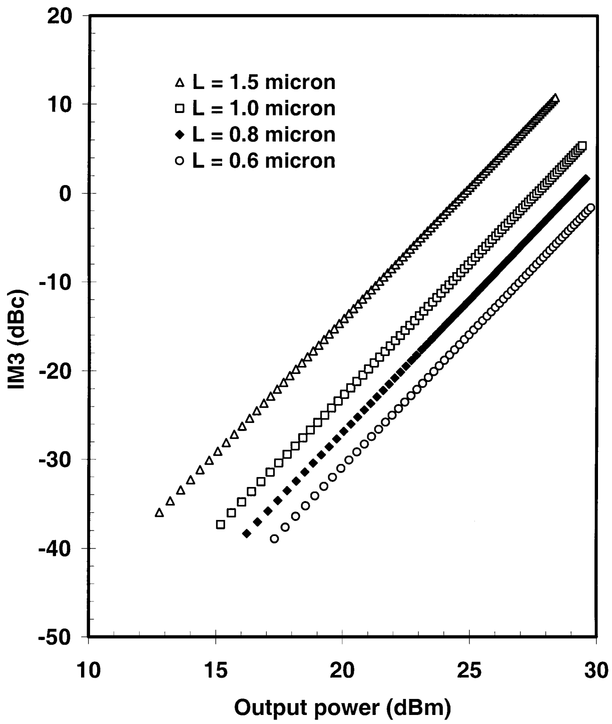

Fig. 7. IM3 as a function of output power of $L \times 150$ μm GaN MESFETs ($V_{\rm GS} = -4$ V and $V_{\rm DS} = 25$ V) [12].

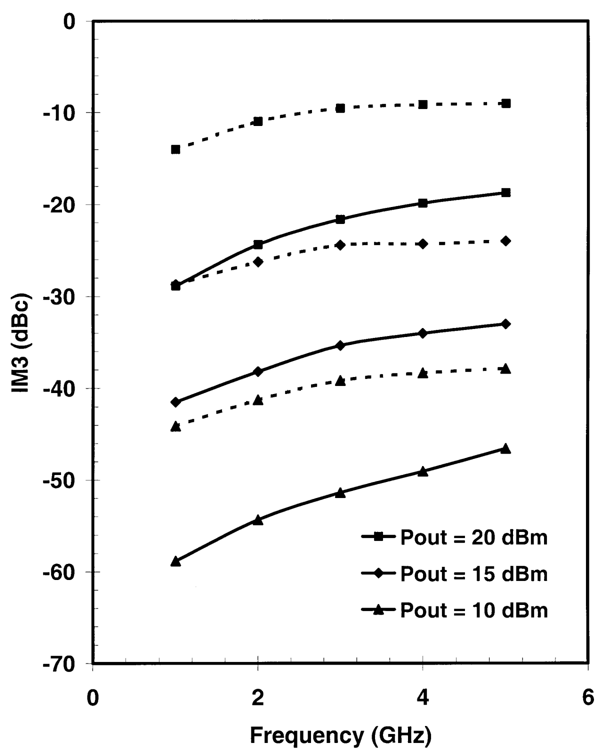

Fig. 8. IM3 as a function of frequency with output power as a parameter. Devices are 0.6 μm × 150 μm (solid lines) and 1.5 μm × 150 μm (dashed lines) GaN MESFETs ($V_{\rm GS} = -4$ V and $V_{\rm DS} = 25$ V) [12].

Fig. 8 shows IM3 as a function of principal tone frequency with output power as a parameter. The second tone is assumed 10 MHz higher than the principal tone frequency. It is observed that IM3 increases with increasing frequency for a given output power level. This is attributed to the third-order transfer function $|H_3(\omega_1, \omega_1, -\omega_2)|$, which increases with decreasing capacitive reactance due to $C_{\rm gd}$, and the first-order transfer function $|H_1(\omega_1)|$, which decreases with decreasing capacitive reactance due to $C_{\rm gs0}$, as evident from (21). Moreover, at a given frequency, IM3 increases with an increasing gate length and output power level. For structures with longer gate lengths, higher IM3 is obtained due to higher capacitances and lower transconductances (see Table I). At elevated output power levels, device nonlinearity increases, which results in higher IM3.

IV. Conclusion

Nonlinearities of GaN MESFETs are reported using a Volterra-series technique. A physics-based large-signal model is used to include the frequency dispersion of transconductance and output resistance due to the presence of traps. Calculated *I–V* characteristics are in good agreement with experimental data. The calculated f_T and $f_{\max}$ are in excellent agreement with the experimental data. A significant improvement in device linearity is observed for shorter gatelength devices at lower operating frequencies.

Appendix
Circuit Parameters for the Trapping Related Sub-Network

The trapping sub-network parameters are given by [14], [15]

$$g_m'' = qv_{\rm sat}WdN_{\rm to}\alpha\left[\frac{a_1 + 2a_2V_{\rm GS}}{1 + a_1 + 2a_2V_{\rm GS}}\right] \times \exp\left[-\alpha\left(V_{\rm DS} - V_{\rm DS}^{\rm ONSET}\right)\right]$$

$$R_{\rm ds}'' \approx \frac{t_d}{C_{\rm ss}(1 + g_{m2}R_{\rm ds1})}$$

$$C_{\rm ss} \approx C_{\rm gs}$$

where $V_{\rm DS}^{\rm ONSET} = a_0 + a_1V_{\rm GS} + a_2V_{\rm GS}^2, a_0 = 6.24$ V, $a_1 = 1.29$, and $a_2 = 0.03$ V^{-1}.

References

[1] Y. Ohno and M. Kuzuhara, "Application of GaN-based heterojunction FETs for advanced wireless communication," *IEEE Trans. Electron Devices*, vol. 48, pp. 517–523, Mar. 2001.
[2] U. K. Mishra, Y.-F. Wu, B. P. Keller, S. Keller, and S. P. Denbaars, "GaN microwave electronics," *IEEE Trans. Microwave Theory Tech.*, vol. 46, pp. 756–761, June 1998.
[3] W. Lu, J. Yang, M. A. Khan, and I. Adesida, "AlGaN/GaN HEMTs on SiC with over 100 GHz f_T and low microwave noise," *IEEE Trans. Electron Devices*, vol. 48, pp. 581–585, Mar. 2001.
[4] Y.-F. Wu, D. Kapolnek, J. Ibbetson, P. Parikh, B. Keller, and U. K. Mishra, "Very high power density AlGaN/GaN HEMTs," *IEEE Trans. Electron Devices*, vol. 48, pp. 586–590, Mar. 2001.
[5] I. Daumiller, C. Kirchner, M. Kamp, K. Ebeling, L. Pond, C. E. Weitzel, and E. Kohn, "Evaluation of AlGaN/GaN HFET's up to 750°C," in *Proc. Device Res. Conf.*, 1998, pp. 114–115.
[6] A. Ahmed, S. S. Islam, and A. F. M. Anwar, "A temperature dependent nonlinear analysis of GaN/AlGaN HEMTs using Volterra series," *IEEE Trans. Microwave Theory Tech.*, vol. 49, pp. 1518–1524, Sept. 2001.
[7] S. S. Islam and A. F. M. Anwar, "Temperature dependent nonlinearities in GaN/AlGaN HEMTs," *IEEE Trans. Electron Devices*, vol. 49, pp. 710–717, May 2002.
[8] J. M. Golio, M. G. Miller, G. N. Maracas, and D. A. Johnson, "Frequency-dependent electrical characteristics of GaAs MESFETs," *IEEE Trans. Electron Devices*, vol. 37, pp. 1217–1227, May 1990.

[9] T. Ytterdal, T. A. Fjedly, M. S. Shur, S. M. Baier, and R. Lucero, "Enhanced heterostructure field effect transistor CAD model suitable for simulation of mixed-mode circuits," *IEEE Trans. Electron Devices*, vol. 46, pp. 1577–1588, Aug. 1999.
[10] S. C. Binari, K. Ikossi, J. A. Roussos, W. Kruppa, D. Park, H. B. Dietrich, D. D. Koleske, A. E. Wickenden, and R. L. Henry, "Trapping effects and microwave power performance in AlGaN/GaN HEMTs," *IEEE Trans. Electron Devices*, vol. 48, pp. 465–477, Mar. 2001.
[11] Y.-M. Hsin, H.-T. Hsu, C.-C. Chuo, and J.-I. Chyi, "Device characteristics of the GaN/InGaN-doped channel HFETs," *IEEE Electron Device Lett.*, vol. 22, pp. 501–503, Nov. 2001.
[12] S. C. Binari, W. Kruppa, H. B. Dietrich, G. Kelner, A. E. Wickenden, and J. A. Freitas, Jr., "Fabrication and characterization of GaN FETs," *Solid State Electron.*, vol. 41, no. 10, pp. 1549–1554, Oct. 1997.
[13] K. Kunihiro, K. Kasahara, Y. Takahashi, and Y. Ohno, "Experimental evaluation of impact ionization coefficients in GaN," *IEEE Electron Device Lett.*, vol. 20, pp. 608–610, Dec. 1999.
[14] S. S. Islam, "Large-signal modeling of GaN-based microwave power transistors," Ph.D. dissertation, Dept. Elect. Eng., Univ. Connecticut, Storrs, CT, 2002.
[15] S. S. Islam and A. F. M. Anwar, "Large-signal modeling of GaN FET and nonlinearity analysis using Volterra series," in *Proc. IEEE RFIC Symp. Dig.*, 2002, pp. 267–270.
[16] A. M. Crosmun and S. A. Mass, "Minimization of intermodulation distortion in GaAs MESFET small-signal amplifiers," *IEEE Trans. Microwave Theory Tech.*, vol. 37, pp. 1411–1417, Sept. 1989.
[17] J. Lee, W. Kim, Y. Kim, T. Rho, and B. Kim, "Intermodulation mechanism and linearization of AlGaAs/GaAs HBT," *IEEE Trans. Microwave Theory Tech.*, vol. 45, pp. 2065–2072, Dec. 1997.
[18] S. A. Mass, *Nonlinear Microwave Circuits*. Norwood, MA: Artech House, 1988.

Syed S. Islam (S'00) received the B.S. degree in electrical and electronic engineering from the Bangladesh University of Engineering and Technology (BUET), Dhaka, Bangladesh, in 1993, the M.S. degree in electrical engineering from the University of Saskatchewan, Saskatoon, SK, Canada, in 2000, and the Ph.D. degree in electrical engineering from the University of Connecticut, Storrs, in 2002.

He is currently an Assistant Professor with the Department of Electrical Engineering, Rochester Institute of Technology, Rochester, NY. His research interests include numerical techniques, modeling of microwave and millimeter-wave semiconductor devices, and design of microwave amplifiers.

Dr. Islam is a member of the IEEE Electron Devices Society and the IEEE Microwave Theory and Techniques Society (IEEE MTT-S).

A. F. M. Anwar (S'86–M'88–SM'00) received the B.S. and M.S. degrees in electrical and electronic engineering from the Bangladesh University of Engineering and Technology (BUET), Dhaka, Bangladesh, in 1982 and 1984, respectively, and the Ph.D. degree from Clarkson University, Potsdam, NY, in 1988.

He is currently a Professor in the Department of Electrical and Computer Engineering, University of Connecticut, Storrs. His research group, which is within the RF Microelectronics and Noise Laboratory, is currently involved in the study of transport in short heterostructures and antimony based HEMTs operating above 300 GHz. Moreover, the group is involved in modeling GaN-based high-power HEMTs and HBTs. His research activities include the areas of CMOS-based class-E amplifiers, as well as transport dynamics and noise in resonant tunneling diodes (RTDs) and one-dimensional (1-D) structures.

Dr. Anwar is an editor for the IEEE TRANSACTIONS ON ELECTRON DEVICES.